Supporting Information

Ultrarapid and efficient sequestration of iodate and iodide with a pillar[5]arene-based cationic polymeric network

Yongjie Jiang,[‡a] Yue Qi,[‡a] Chengkan Yu,[a] Liancheng Hu,[a] Qing Li,[b] Xiaowei Li,[a] Yimin Cai,*[a] Lihua Yuan,[a] and Wen Feng*[a]

a. Key Laboratory of Radiation Physics and Technology of the Ministry of Education, Institute of Nuclear Science and Technology, College of Chemistry, Sichuan University, Chengdu 610064, China.

b. Biotechnology and Nuclear Technology Research Institute, Sichuan Academy of Agricultural Sciences, Chengdu 610061, China.

‡. These authors contributed equally to this work.

Table of contents

1. Materials and general methods

Materials.

1,4-dibromobenzene, cuprous iodide (CuI), *N,N*-dimethylglycine, 1,4-dibromobutane, hydroquinone, and other reagents involved in synthesis were obtained from Energy Chemical Co. Ltd (Shanghai, China). Sodium chloride, sodium nitrate, sodium carbonate, sodium sulfate, phosphoric acid, potassium iodide (KI), and potassium iodate (KIO_3) used in this work were obtained from Chengdu Forest Science and Technology Development Co., Ltd. All reagents used in this work were of analytical grade without further purification.

Characterization.

^{1}H NMR spectra were collected on a Bruker AVANCE III HD-400 MHZ. Solid-state cross-polarization magic angle spinning (CP/MAS) ^{13}C NMR spectrum was obtained with a Bruker AVANCE III 500MHz with a wide bore Bruker 4 mm broadband (BB)/1H MAS probe. The MAS spin rate was set to 10 Khz, and the pulse program for acquisition is cp. Fourier transform infrared (FT-IR) data in the range of 400-4000 cm^{-1} were recorded on a Bruker ALPHA infrared spectrometer. Thermogravimetric analysis (TGA) experiment was conducted on a DTG-60(H) at a rate of 10 °C/min under nitrogen atmosphere. Powder X-ray diffraction (PXRD) pattern was collected on Schimadzu-XRD6100 and DX-2700 diffractometer. Scanning electron microscopy (SEM) and energy-dispersive X-ray spectroscopy (EDS) were studied on a ZEISS Gemini 300 microscope. Transmission electron microscopy (TEM) images were recorded using JEMF200 at an accelerating voltage of 200 kV. X-ray photoelectron spectroscopy (XPS) was studied with an AXIS SUPRA+ photoelectron spectrometer. Dynamic light scattering (DLS) experiments were measured using a Zetasizer Nano ZS90 instrument in a quartz cuvette, and the measurements were performed in water. An UV-vis spectrophotometer (UV-3600i Plus, Shimadzu, Japan) was used for collecting UV-vis spectra. The accurate concentrations of iodate and iodide were measured by inductively coupled plasma optical emission spectroscopy (ICP-OES, PerkinElmer, ICP optima 8000). The water contact angle (CA) was measured on Data

physics OCA40.

I^-/IO_3^- adsorption.

Nonradioactive iodine isotope was used instead of radioiodine due to their identical chemical properties. A fixed amount of adsorbent was added to a series of KI and KIO_3 solutions. Afterward, the solids and solutions were separated by filtration, and the solutions were measured by UV-vis spectroscopy to determine the concentration of I^- anion according to the density at 226 nm.

IO_3^- concentrations were determined by the absorbance of triiodide (I_3^-).[1] IO_3^- was converted to I_3^- by the reaction of iodate with iodide in acidic environment as shown below:

$$IO_3^- + 5I^- + 6H^+ \rightarrow 3I_2 + 3H_2O$$

$$I_2 + I^- \rightarrow I_3^-$$

1 mL of 0.1 M H_3PO_4 and 1 mL of 2% KI were successively added to 2 mL of IO_3^- solutions and the resulting samples were measured by UV-vis spectroscopy to determine the concentration of I_3^- according to the density at 350 nm.

Adsorption isotherms study.

The adsorption isotherms were investigated by carrying out adsorption experiments with I^- or IO_3^- solutions of increasing concentrations from 50 to 1000 ppm. The adsorbent was immersed into iodine solutions at a solid-liquid ratio of 0.5 g/L. The resulting mixture was shaken for 12 hours, and then the aqueous phase was separated by a 0.22 μm membrane. The adsorption capacity was calculated based on the following equation (1):

$$q_e = \frac{(C_0 - C_e)V}{m} \quad (1)$$

where q_e (mg g^{-1}) is the adsorption capacity at equilibrium. C_0 (mg L^{-1}) and C_e (mg L^{-1}) are the initial concentration and equilibrium concentration of I^- or IO_3^-, respectively. V (L) is the volume of the solution and m (g) is the mass of the adsorbent. The adsorption isotherms of P5-CPN, P5-CPN-Br and MP-CPN for iodate and iodide were analyzed using the Langmuir and Freundlich isotherm models as described below:

Langmuir isotherm model：

$$\frac{C_e}{q_e} = \frac{C_e}{q_m} + \frac{1}{K_L q_m} \quad (2)$$

Freundlich isotherm model：

$$ln\, q_e = ln\, K_F + \frac{1}{n} ln\, C_e \quad (3)$$

where q_m (mg g^{-1}) stands for the maximum adsorption capacity. K_L (L mg^{-1}) is the Langmuir constant, which is related to the binding affinity. K_F (mg^{1-n} $L^{1/n}$ g^{-1}) and n are the Freundlich constants related to sorption capacity and sorption intensity, respectively.

Adsorption kinetics study.

The adsorption kinetics experiments of P5-CPN and MP-CPN for I^- and IO_3^- were completed by stirring the material in iodine solutions at room temperature. Specifically, 50 mg of P5-CPN or MP-CPN was added to 50 mL of solutions with the initial iodine concentration of 500 mg L^{-1}. The resulting mixture was stirred for different contact times (30 s, 1 min, 2 min, 4 min, 8 min, 15 min, 30 min, 60 min, 120 min, and 240 min), after which the aqueous phase was separated by a 0.22 μm membrane, and the filtrate was analyzed by UV-vis spectroscopy. The removal efficiency (R_e) and distribution coefficient (K_d) were calculated based on equations:

$$R_e = \frac{C_0 - C_e}{C_0} \times 100\% \quad (4)$$

$$K_d = \frac{V(C_0 - C_e)}{mC_e} \quad (5)$$

The adsorption kinetics data were fitted by the pseudo-first-order and pseudo-second-order models expressed as follows:

Pseudo-first-order model:

$$ln(\, q_e - q_t) = ln\, q_e - k_1 t \quad (6)$$

Pseudo-second-order model:

$$\frac{t}{q_t} = \frac{1}{k_2 {q_e}^2} + \frac{t}{q_e} \quad (7)$$

where k_1 (min^{-1}) and k_2 ($g\ mg^{-1}\ min^{-1}$) represent the rate constants of the pseudo-first-order model and pseudo-second-order model, respectively. q_t (mg g^{-1}) and q_e (mg g^{-1}) refer to the adsorption capacities at a certain contact time t (min) and equilibrium, respectively.

Effect of pH.

To explore the effect of pH value on adsorption capacity towards I^- and IO_3^-, batch experiments were conducted with 500 mg L^{-1} I^- or IO_3^- solutions of pH values ranging from 3 to 11. The pH of the solution was adjusted using NaOH and/or HNO_3 solutions. The solid-liquid ratio was 1 g/L. After the mixture was shaken for 12 hours, the aqueous phase was separated by a 0.22 μm membrane, and the filtrate was analyzed by UV-vis spectroscopy.

Selectivity study.

The selectivity of P5-CPN was evaluated by investigating its removal efficiency toward I^- and IO_3^- in the presence of competing anions (Cl^-, SO_4^{2-}, NO_3^-, and CO_3^{2-}). Adsorption experiments were conducted with a solution containing 5 mg L^{-1} I^- or IO_3^- at a solid-liquid ratio of 1 g/L and the concentration ratio of I^- or IO_3^- to competitive anion is 1:1. The mixture was shaken for 12 hours, followed by separating the aqueous phase with a 0.22 μm membrane. The concentration of residual I^- or IO_3^- was analyzed by UV-vis spectroscopy.

Radiation stability tests.

P5-CPN was irradiated with γ-rays (^{60}Co source) at doses of 100, 200, 400, and 500 kGy. Irradiated P5-CPN was contacted with a 500 mg L^{-1} I^- or IO_3^- solution at a solid-liquid ratio of 1 g/L to assess its adsorption performance. The concentration of residual I^- or IO_3^- was analyzed by UV-vis spectroscopy.

Reusability study.

To evaluate the recycling performance, the adsorbent was initially contacted with a 50 mg L^{-1} iodine solution at a solid-liquid ratio of 1 g/L. Subsequently, the adsorbent loaded with I^- or IO_3^- was immersed in a 3M NaCl solution and shaken at 25 °C for 12 hours. The adsorbent was then filtered, washed with water, and dried at 60 °C for 12 h. The resulting mixture was separated by a 0.22 μm membrane, and the filtrate was analyzed by UV-vis spectroscopy. The adsorption-desorption experiments were repeated for five cycles.

Adsorption in simulated Hanford groundwater.

The simulated Hanford groundwater was prepared according to the reported protocol.[2]

The iodine concentration is *ca.* 1 mg L^{-1}. P5-CPN was added into simulated Hanford groundwater with the solid-liquid ratios of 0.5, 1, 2, and 5 g/L, respectively. After the mixture was shaken for 12 h, the aqueous phase was separated by a 0.22 μm membrane and the accurate concentration of residual IO_3^- or I^- was detected by ICP-OES.

Dynamic adsorption experiments.

To evaluate the potential of P5-CPN for industrial applications, dynamic adsorption experiments were conducted. Simulated Hanford groundwater (SGW) containing I^- or IO_3^- was passed through a column filled with a mixture of P5-CPN and silica gel as the packing material. The SGW solution was pumped into the column at a flow rate of 1 mL min^{-1} and the accurate concentration of IO_3^- or I^- in the effluent was detected by ICP-OES.

Computational method.

Density functional theory (DFT) calculations were carried out using Gaussian 09 software.[3] The fragment PM was employed as a model to simulate the structure of P5-CPN. The different structures of PM-A^- (A = IO_3^-, I^-, SO_4^{2-}, NO_3^- and Cl^-) and their respective anions were fully optimized at B3LYP level with SDD-6-31G* basis set.[4] To obtain accurate energy information, single-point energy calculations in water were performed at the B3LYP level with SDD-6-311G* basic set and SMD method was used.[5] The adsorption energies (ΔE) were calculated according to the following equation:

$$\Delta E = E(PM - A^-) + E(Cl^-) - E(PM - Cl^-) - E(A^-) \quad (8)$$

where E(PM-A^-), E(Cl^-), E(PM-Cl^-), and E(A^-) indicate the total energies of PM-A^-, Cl^-, PM-Cl^-, and A^-, respectively.

2. Synthesis

Synthesis of 1,4-Bis (1-imidazolyl) benzene (BIB).[6]

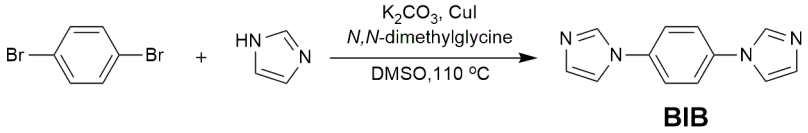

Scheme S1. Synthesis of BIB.

1,4-dibromobenzene (4.67 g, 20.0 mmol), imidazole (3.35 g, 50.0 mmol), *N,N*-dimethylglycine (0.835 g, 8.10 mmol), CuI (0.817 g, 4.30 mmol), and K_2CO_3 (11.1 g, 80.4 mmol) were dissolved in 50 mL of DMSO. The reactant was then heated at 110 °C and stirred for 48 h under nitrogen atmosphere. The mixture was cooled to room temperature, and water and ethyl acetate were added to the mixture. The organic phase was separated and the aqueous phase was extracted with ethyl acetate for three times. The combined organic phase was washed with brine, dried over anhydrous magnesium sulfate, and concentrated in vacuo. The crude product was filtered and the white precipitate was purified by silica gel column chromatograph with methanol and CH_2Cl_2 (2:8, v/v) as the eluent to afford BIB as a white powder (2.47 g, 53 %). ^{1}H NMR (400 MHz, $CDCl_3$) δ 7.88 (s, 2H), 7.53 (s, 4H), 7.31 (s, 2H), 7.25 (s, 2H).

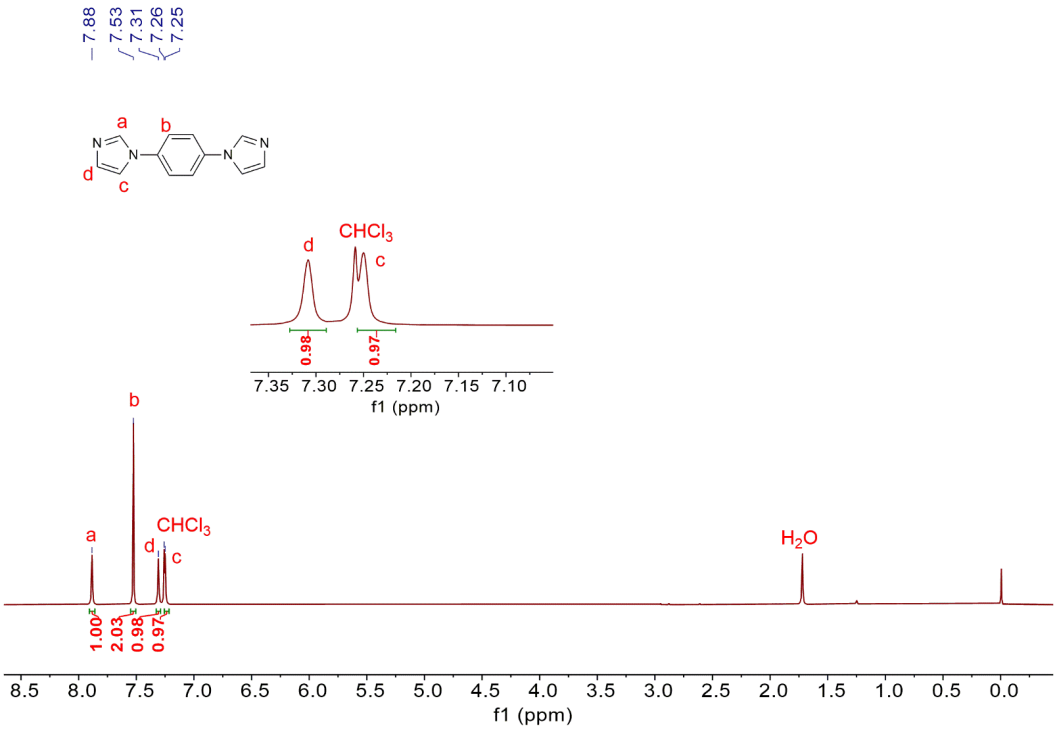

Fig. S1 ^{1}H NMR spectrum of BIB (400 MHz, $CDCl_3$, 298K).

Synthesis of P5-Br.[7]

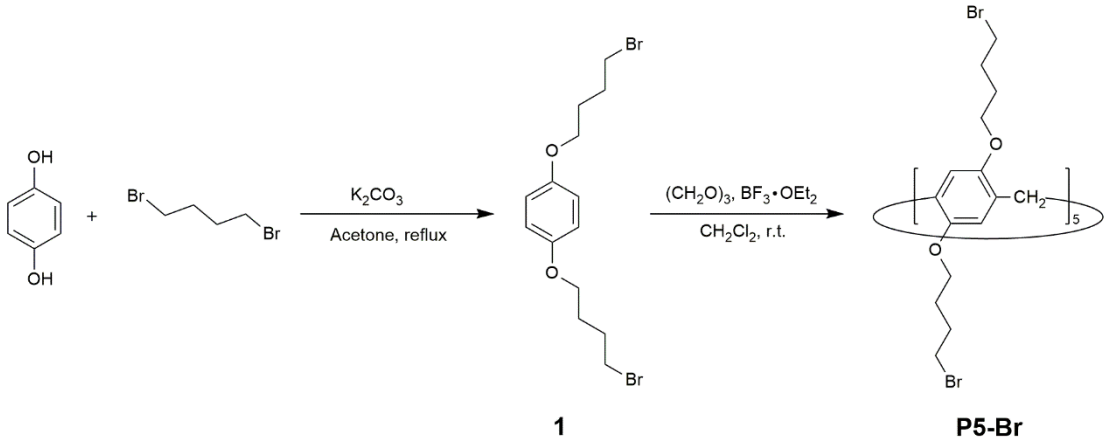

Scheme S2. Synthesis of P5-Br.

Synthesis of Compound 1.

1,4-dibromobutane (0.864 g, 4.00 mmol) was added to a solution of K_2CO_3 (0.138 g, 1.00 mmol) and hydroquinone (0.110 g, 1.00 mmol) in acetone (200 mL). The mixture was heated to reflux under nitrogen atmosphere for 72 h. The solid was filtered off and the solvent was removed under vacuum. The residue was recrystallized in dichloromethane and petroleum ether. The compound **1** was collected by filtration (0.360 g, 95 %). ^{1}H NMR (400 MHz, $CDCl_3$) δ (ppm): 6.81 (s, 4 H), 3.94 (t, J = 6.4 Hz, 4 H), 3.49 (t, J = 6.8 Hz, 4 H), 2.08-1.2.03 (m, 4 H), 1.95-1.90 (m, 4 H).

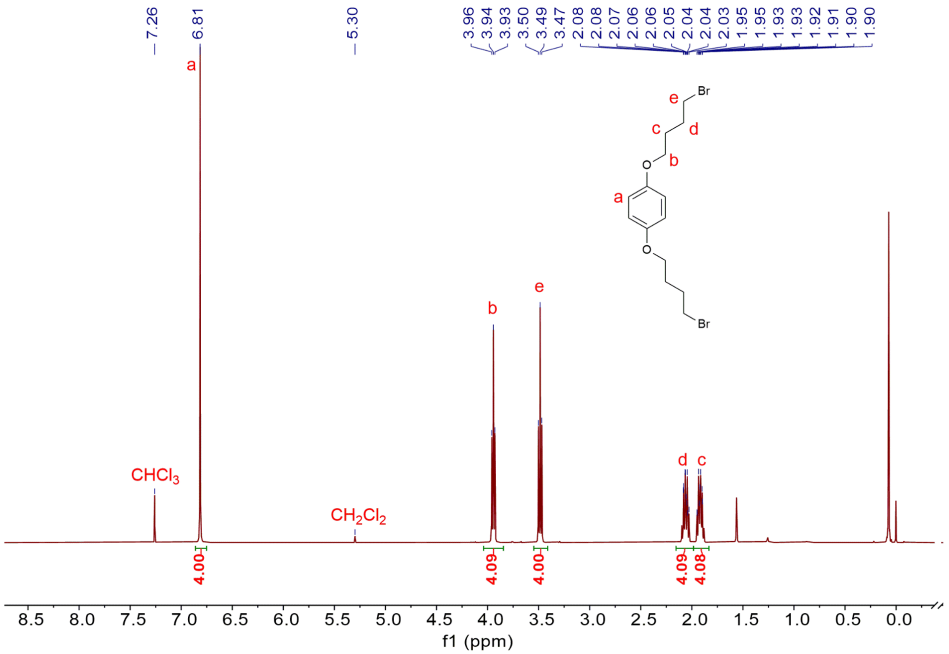

Fig. S2 ^{1}H NMR spectrum of **1** (400 MHz, $CDCl_3$, 298K).

Synthesis of P5-Br.

To a solution of **1** (3.03 g, 9.34 mmol) in dry dichloromethane (80 mL) was added 1,3,5-trioxane (0.280 g, 3.11 mmol) under nitrogen atmosphere. Boron trifluoride diethyl etherate (1.32 g, 11.5 mmol) was then added to the solution and the mixture was stirred at room temperature for 1 h. Water (100 mL) was added to quench the reaction. The organic layer was washed with H_2O (100 mL × 3) and dried over anhydrous magnesium sulfate. The solvent was removed under reduced pressure. The obtained solid was purified by silica gel column chromatograph with petroleum ether/dichloromethane (1:1, v/v) as the eluent to afford a white powder (1.21 g, 40 %). ^{1}H NMR (400 MHz, $CDCl_3$) δ (ppm): 6.83 (s, 10 H), 3.94 (t, J = 6 Hz, 20 H), 3.76 (s, 10 H), 3.45 (t, J = 6.4 Hz, 20 H), 2.09-2.03 (m, 20 H), 1.97-1.92(m, 20 H).

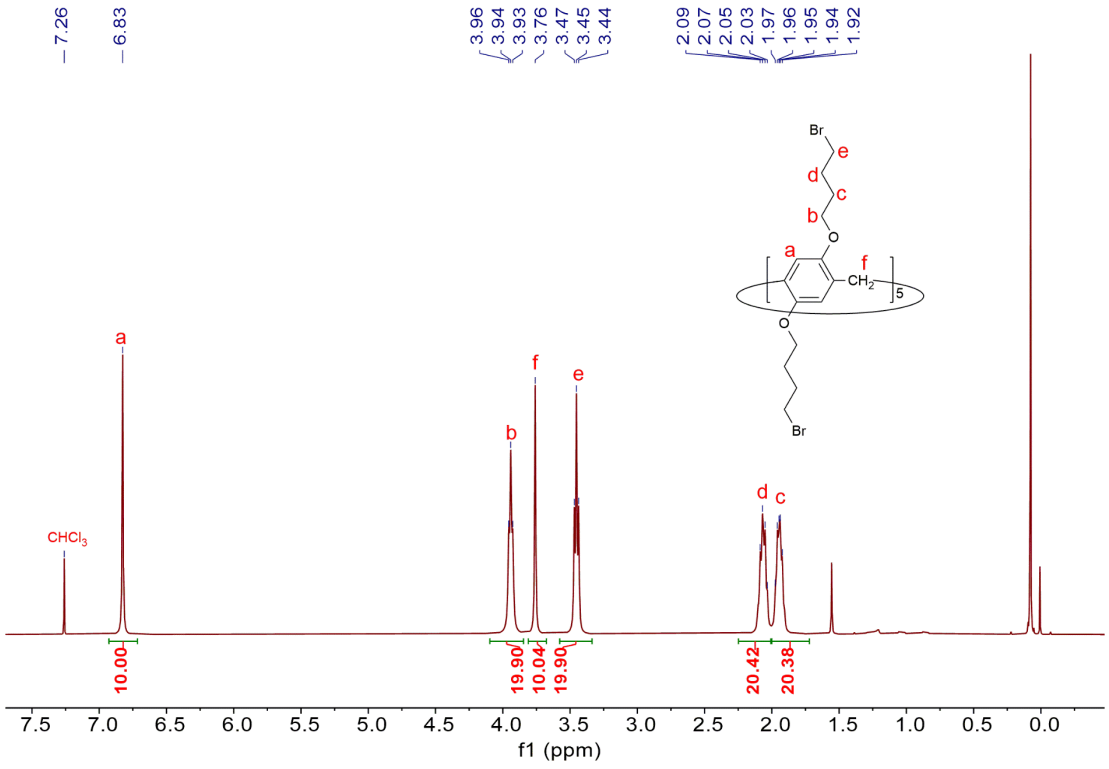

Fig. S3 ^{1}H NMR spectrum of P5-Br (400 MHz, $CDCl_3$, 298K).

Synthesis of P5-CPN.

1.00 g (0.510 mmol) of P5-Br and 0.536 g (2.55 mmol) of BIB were added to 100 mL of DMF. The resulting mixture was then heated at 120 °C and stirred for 3 days under N_2 atmosphere. After cooling to room temperature, the crude product was obtained by filtration and washed with THF (100 mL × 3) and methanol (100 mL × 3). The resulting

solid was then purified by Soxhlet extraction with methanol/THF (1:1, v/v) for 48 hours to afford a beige powder, which was then immersed in a saturated NaCl solution for 24 hours, followed by washing with water and drying under vacuum at 60 °C for 24 hours to obtain P5-CPN as a beige powder (1.29 g, 91%).

Synthesis of MP-Br.

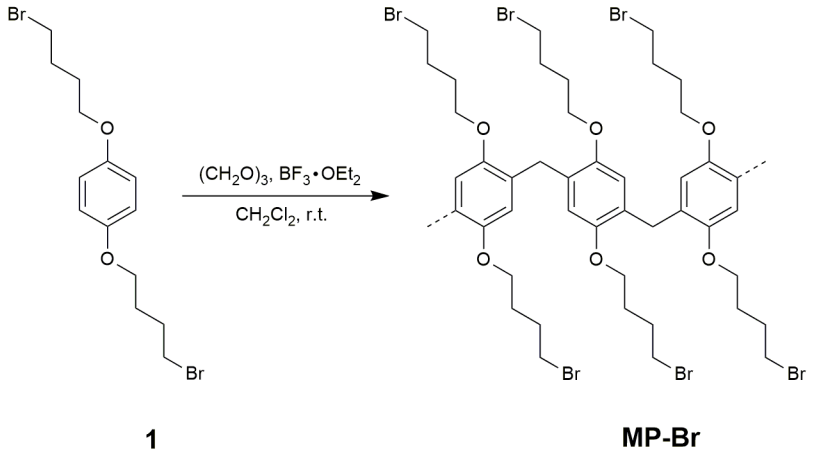

1 **MP-Br**

Scheme S3. Synthesis of MP-Br.

To a solution of **1** (1 g, 3.08 mmol) in dry dichloromethane (20 mL) was added 1,3,5-trioxane (0.093 g, 1.04 mmol) under nitrogen atmosphere. Boron trifluoride diethyl etherate (1.32 g, 11.5 mmol) was then added to the solution and the mixture was stirred at room temperature for 12 h. No P5-Br and compound **1** was detected by TLC monitoring. Water (100 mL) was added to quench the reaction. The organic layer was washed with H_2O (100 mL × 3) and dried over anhydrous magnesium sulfate. The solvent was removed under reduced pressure and the resulting solid was a green powder that was insoluble in all organic solvents. Fourier Transform Infrared (FT-IR) spectroscopy confirmed that the structure of MP-Br is similar to those of compound **1** and P5-Br.

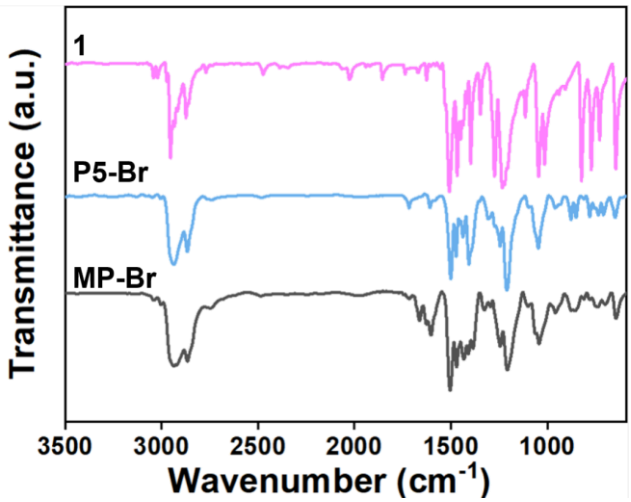

Fig. S4. FT-IR spectra of 1, P5-Br, and MP-Br.

Synthesis of MP-CPN.

0.816 g (2.00 mmol) of MP-Br and 0.421 g (2.00 mmol) of BIB were added to 75 mL of DMF. The resulting mixture was then heated at 120 °C and stirred for 3 days under N_2 atmosphere. After cooling to room temperature, the crude product was obtained by filtration and washed with THF (100 mL × 3) and methanol (100 mL × 3). The resulting solid was purified by Soxhlet extraction with methanol/THF (1:1, v/v) for 48 hours to afford a yellow powder, which was then immersed in a saturated NaCl solution for 24 hours, followed by drying under vacuum at 60 °C for 24 hours to obtain MP-CPN as a yellow powder (0.83g, 75%).

3. Characterization of P5-CPN and MP-CPN

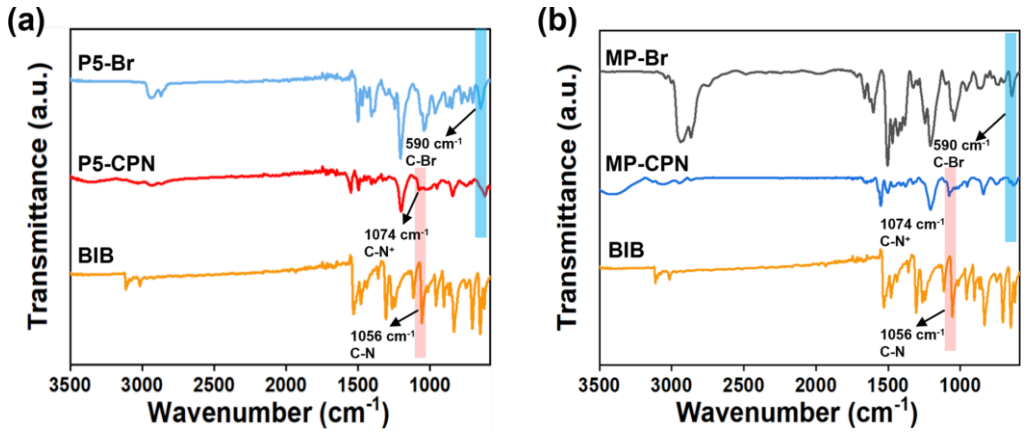

Fig. S5. (a) FT-IR spectra of P5-Br, BIB, and P5-CPN. (b) FT-IR spectra of MP-Br, BIB, and MP-CPN.

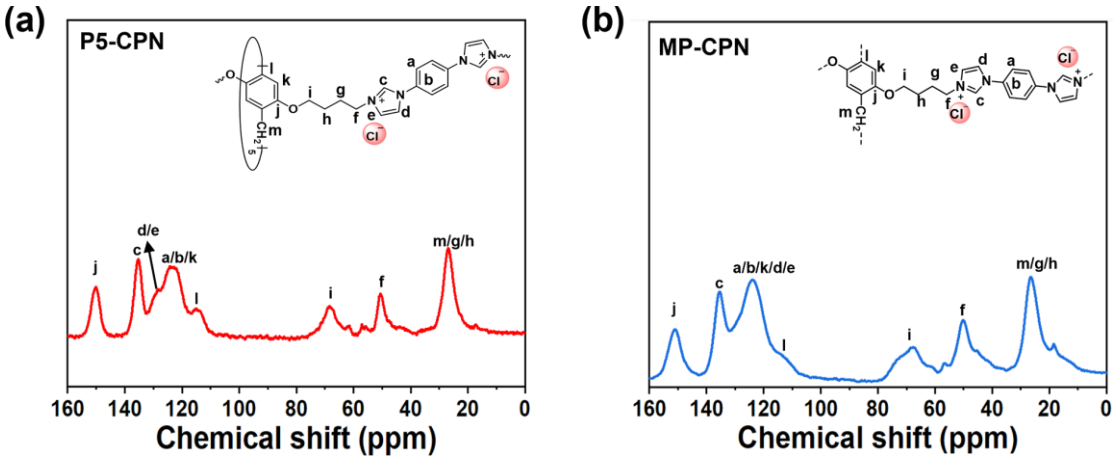

Fig. S6. Solid-state ^{13}C NMR spectra of (a) P5-CPN and (b) MP-CPN.

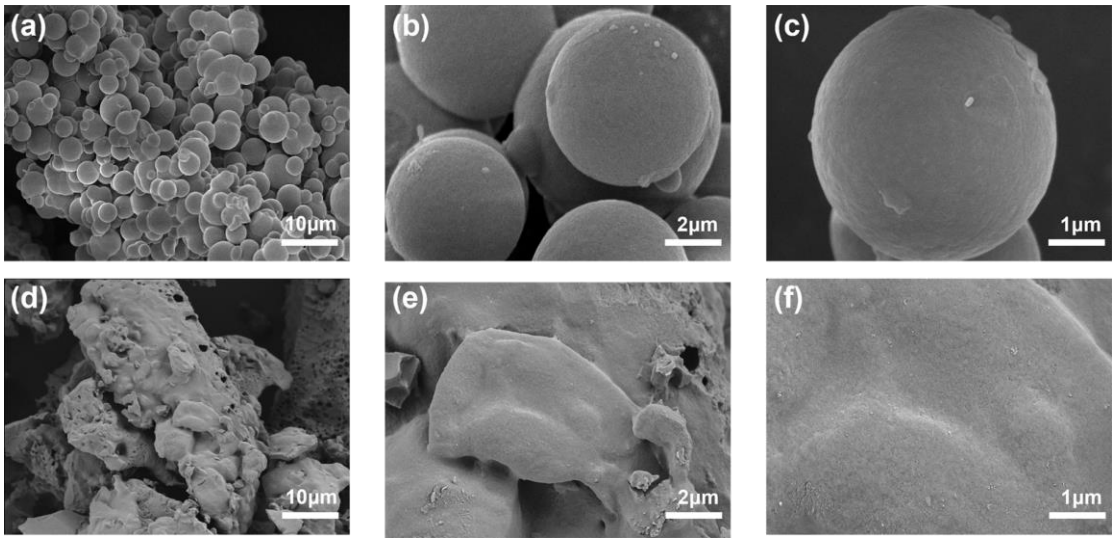

Fig. S7. SEM images of P5-CPN (a-c) and MP-CPN (d-f).

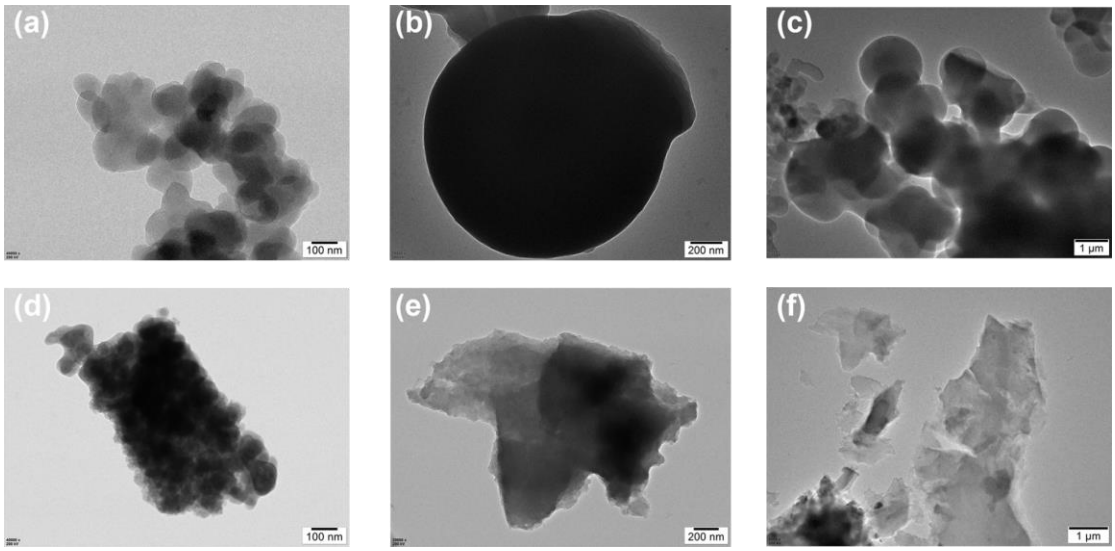

Fig. S8. TEM images of P5-CPN (a-c) and MP-CPN (d-f).

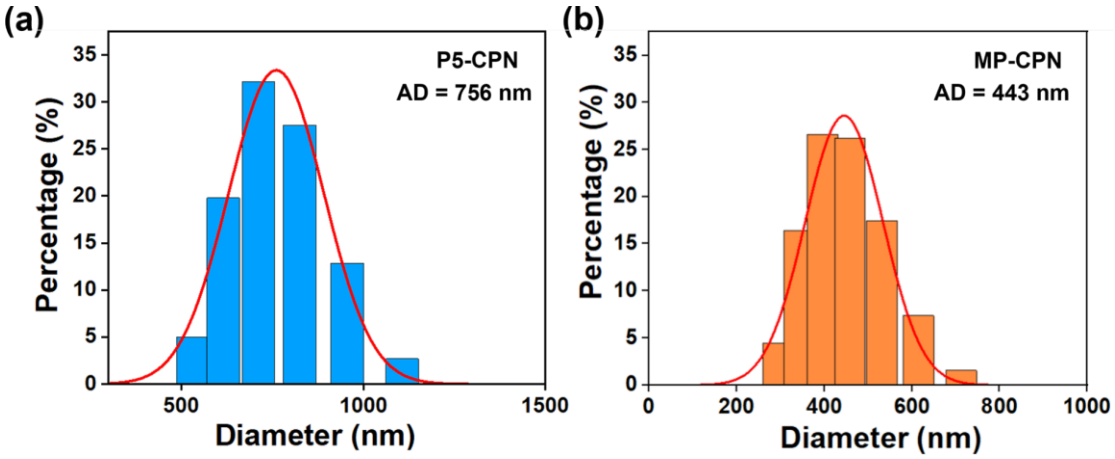

Fig. S9. The DLS profiles of (a) P5-CPN and (b) MP-CPN.

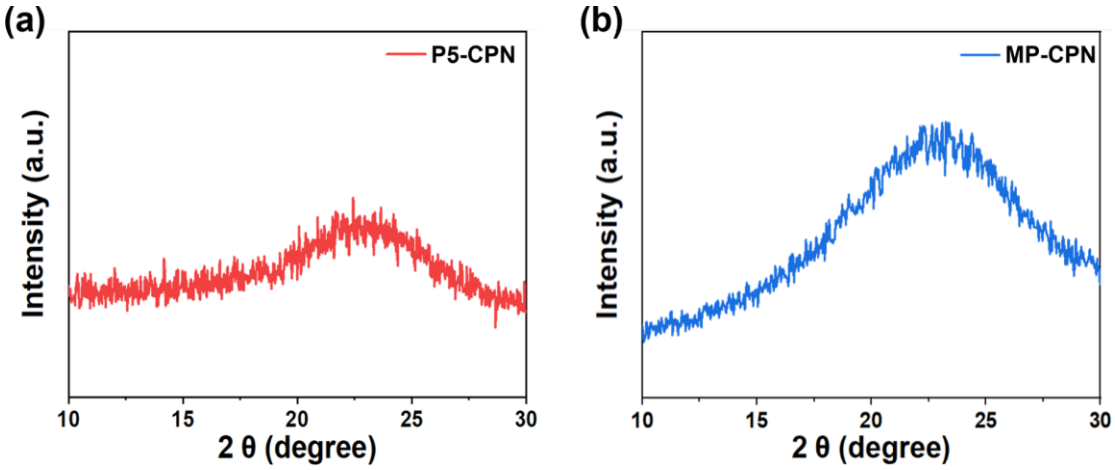

Fig. S10. PXRD patterns of (a) P5-CPN and (b) MP-CPN.

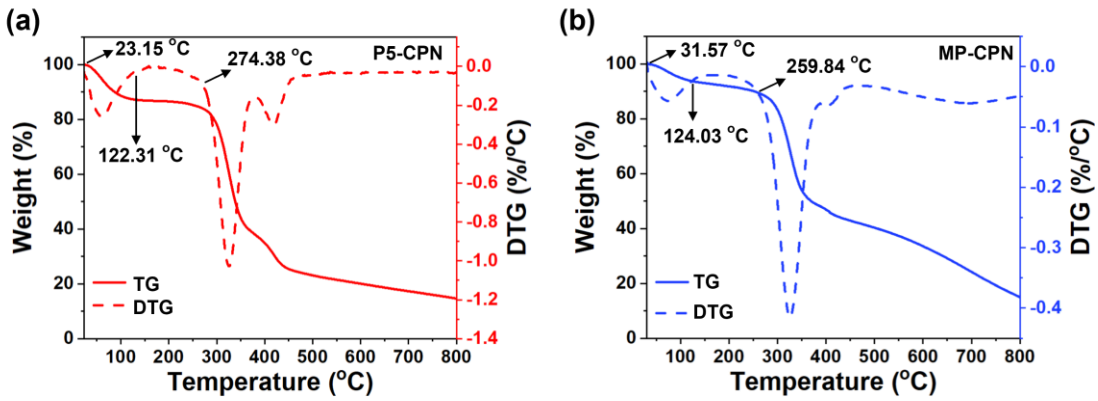

Fig. S11. TGA and DTG curves of (a) P5-CPN and (b) MP-CPN.

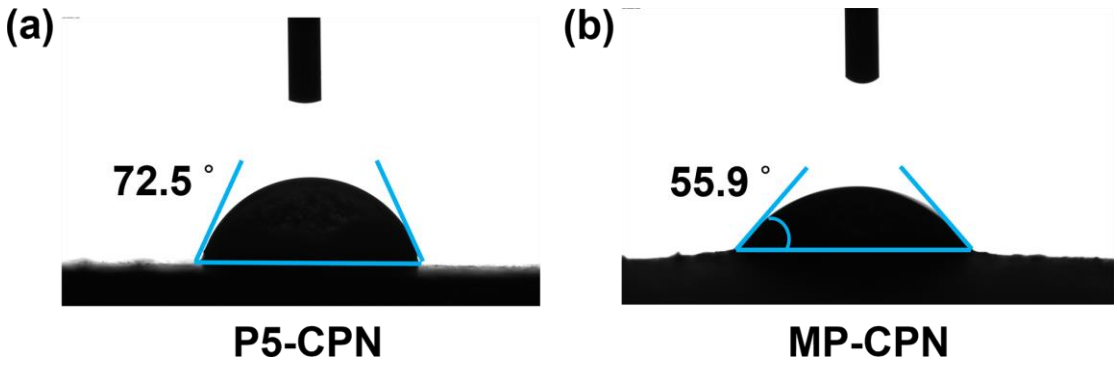

Fig. S12. Contact angles for a water droplet on pressed pellets of (a) P5-CPN and (b) MP-CPN.

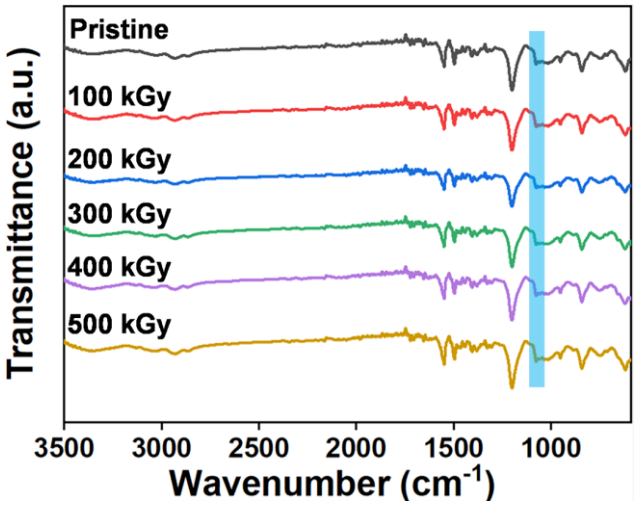

Fig. S13 FT-IR spectra of P5-CPN after γ-irradiation.

4. **Adsorption experiments**

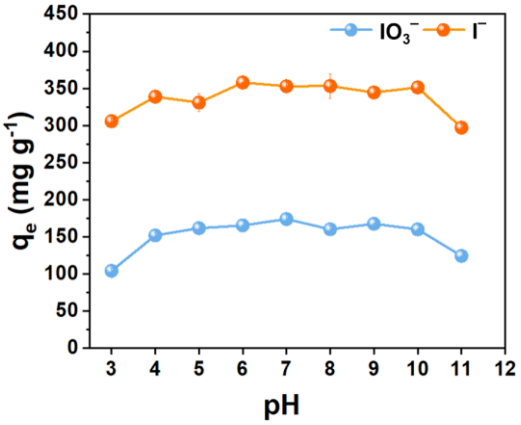

Fig. S14. Effect of pH value on the I^- and IO_3^- sorption by P5-CPN.

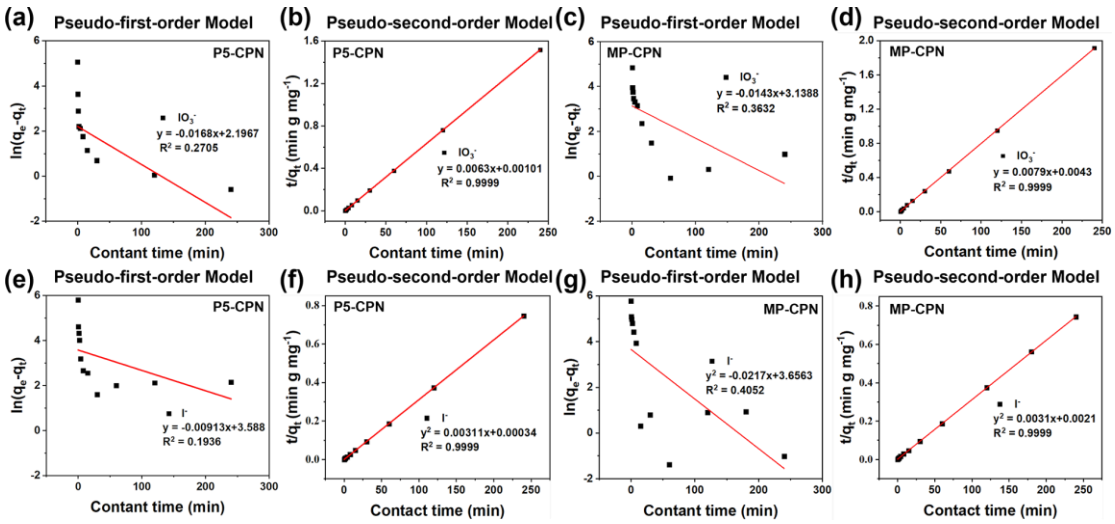

Fig. S15. Pseudo-first-order and pseudo-second-order plots for IO_3^- and I^- adsorption onto P5-CPN and MP-CPN.

Table S1. Fitting results of the kinetics data with pseudo-first-order and pseudo-second-order kinetics models.

		Pseudo-first-order model			**Pseudo-second-order model**		
		q_e (mg g^{-1})	k_1 (min^{-1})	R^2	q_e (mg g^{-1})	k_2 (g mg^{-1} min^{-1})	R^2
P5-CPN	IO_3^-	8.995	0.0168	0.2705	158.7	0.0393	0.9999
	I^-	36.16	0.0091	0.1936	321.5	0.0284	0.9999
MP-CPN	IO_3^-	*23.08*	0.0143	0.3622	126.6	0.0145	0.9999
	I^-	*38.71*	0.0217	0.4052	322.5	0.0045	0.9999

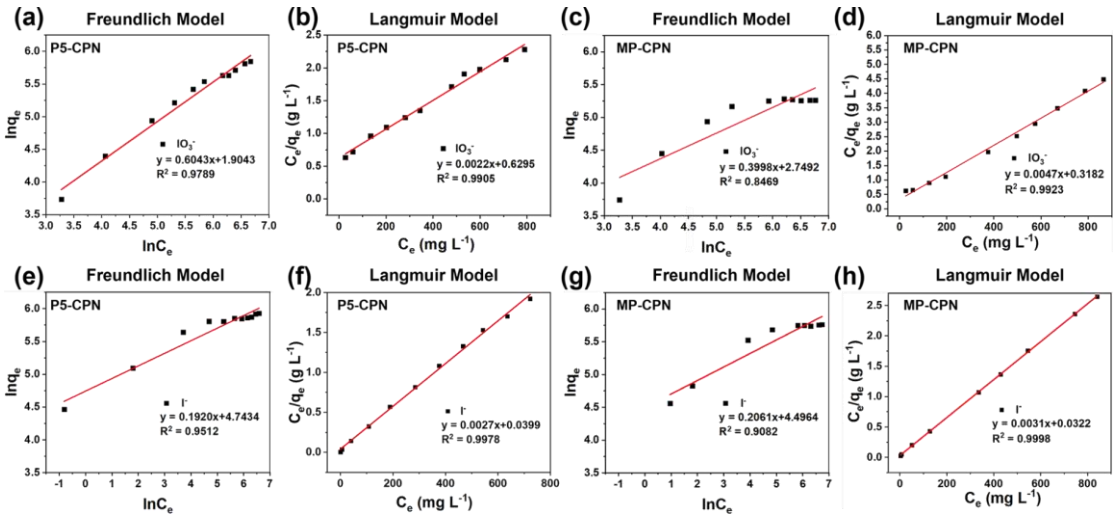

Fig. S16. Freundlich and Langmuir model plots for IO_3^- and I^- adsorption onto P5-CPN and MP-CPN.

Table S2. Fitting results of the isothermal sorption according to the Langmuir and Freundlich models

		Langmuir model			**Freundlich model**		
		q_m (mg g^{-1})	K_L (L mg^{-1})	R^2	n	K_F (mg^{1-n} $L^{1/n}$ g^{-1})	R^2
P5-CPN	IO_3^-	454.5	0.0035	0.9905	1.655	6.714	0.9788
	I^-	370.3	0.0677	0.9978	5.208	114.8	0.9512
MP-CPN	IO_3^-	*212.8*	0.0147	0.9923	2.501	15.63	0.8469
	I^-	*322.6*	0.0962	0.9998	4.852	89.69	0.9052

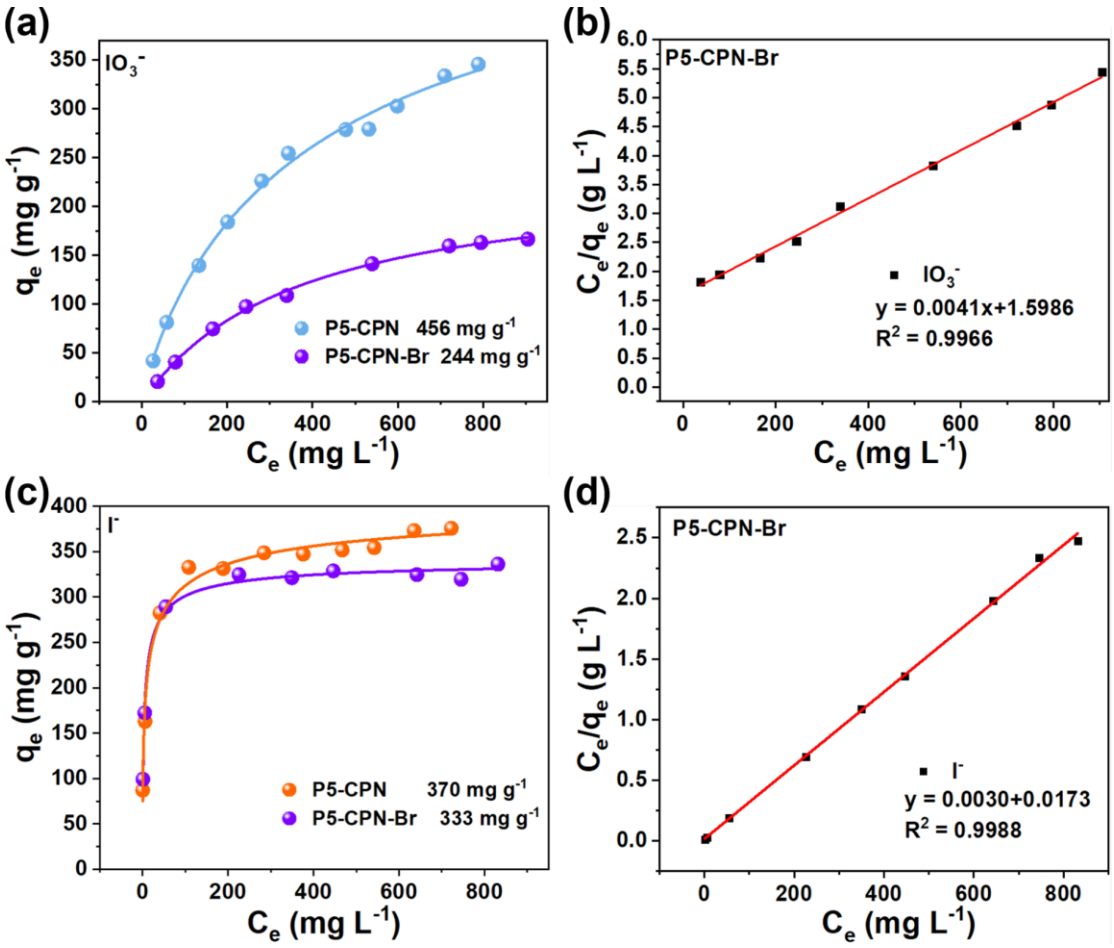

Fig. S17. (a) Adsorption isotherms of P5-CPN and P5-CPN-Br toward IO_3^-. (b) Langmuir model plots for IO_3^- adsorption onto P5-CPN-Br. (c) adsorption isotherms of P5-CPN and P5-CPN-Br toward I^-. (d) Langmuir model plots for I^- adsorption onto P5-CPN-Br.

Table S3. Comparison of the iodate adsorption capacity of P5-CPN with those of reported adsorbents.

Adsorbent	Adsorption capacity ($mg\ g^{-1}$)	Equilibrium time (h)	References
Corn stalk	1.97	120	8
Duckweed	4.056	96	9
Pomelo peel	6.81	96	10
Beishan granite	0.02	12	11
Halloysite	3.9	36	12
Barite	6.07	-	13

Granular activated carbon	30	-	[14]
γ-Al_2O_3	29.58	5	[15]
Ag-zeolite	37	-	[16]
Ag-GAC	0.012	-	[17]
Pyrolytic biochar	10.31	120	[18]
Hydrothermal biochar	16.87	120	[18]
CoCr-4NC	350	1	[19]
CoCr-4C	350	24	[19]
$Bi_2O_{2.33}$	230	0.33	[20]
Cu_2O@CH	313.4	0.5	[21]
δ-Bi_2O_3@PES	170.6	5	[22]
$ZrSbO_2$	612.5	1	[23]
NiAl LDH	395.5	0.33	[24]
CoAl LDH	378	0.33	[24]
MOF-808 (Zr)	233.3	48-72	[25]
Purolite A530E	53.34	1.5	[26]
PB-LDH	91	72	[27]
Mg_2-Al-NO_3 LDH	149.528	4	[28]
SCU-CPN-6	896	2	[1]
P5-CPN	454.5	0.067	This work

Table S4. Comparison of the iodide adsorption capacity of P5-CPN with those of reported adsorbents.

Adsorbent	**Adsorption capacity ($mg\ g^{-1}$)**	**Equilibrium time (h)**	**References**
1.0%-Ag@Cu_2O	25.4	1.5	[29]
Cu/Cu_2O	22.9	5	[30]
MR-δ-Bi_2O_3	182.9	0.25	[31]

Bi_2O_3/LDHs	101.9	1	[32]
Bi@MIL	189.6	0.33	[33]
δ-Bi_2O_3@PES	95.4	300	[22]
BBN-R	454.6	1.5	[34]
Ag/Fe_3O_4	847	3	[35]
Mesoporous δ-Bi_2O_3	364.4	3	[36]
MXene-PDA-Bi_6O_7	64.6	1.5	[37]
Ag_2O@NZU	132	2.6	[38]
SiPyR-N4	149	0.5	[39]
MNP-OMMTs	322.4	1	[40]
Ag_2O-Ag_2O_3/ZIF-8	232.12	0.05	[41]
Cu_2O@CH	416.5	0.5	[21]
CoAl LDH	212.1	0.33	[24]
NiAl LDH	266.7	0.33	[24]
Purolite A530E	275.1	1.5	[26]
microrosette-like δ-Bi_2O_3	182.8	1.5	[31]
CF-AA-Cu	10.32	1	[42]
P5-CPN	370.3	0.067	This work

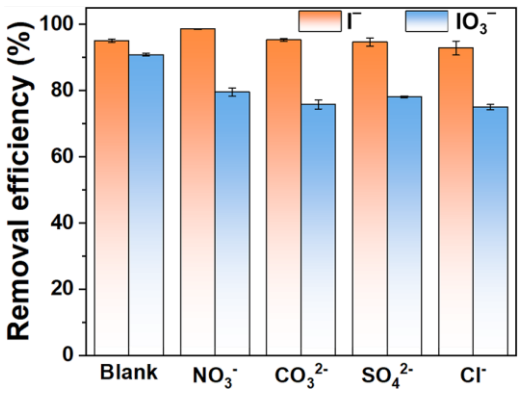

Fig. S18. Effect of different competing anions on I^- and IO_3^- removal by P5-CPN.

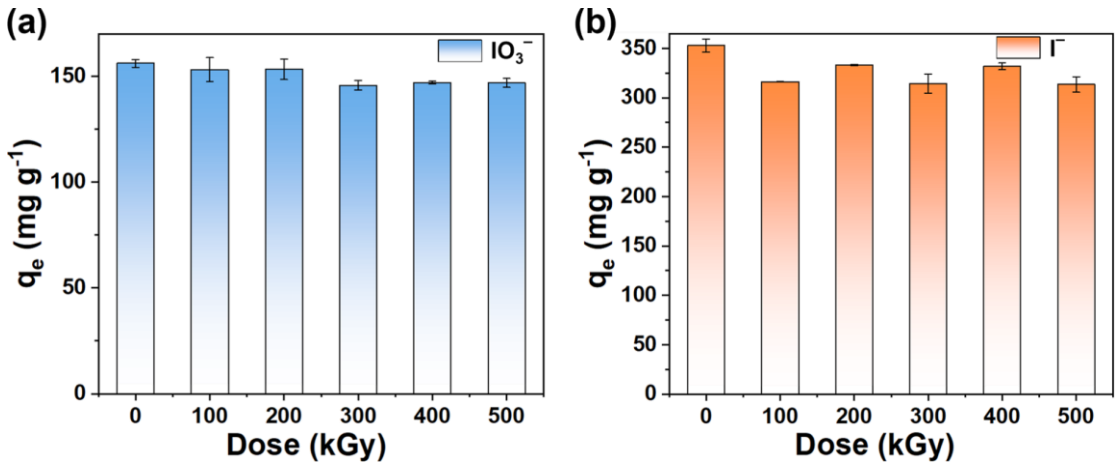

Fig. S19. (a) IO_3^- uptake capacity of P5-CPN before and after being irradiated by γ-rays. (b) I^- uptake capacity of P5-CPN before and after being irradiated by γ-rays.

Table S5. Composition of simulated Hanford groundwater (SGW).

Constituent	Concentration (mg L^{-1})
$H_2SiO_3 \cdot nH_2O$	15.3
KCl	8.20
$MgCO_3$	13.0
NaCl	15.0
$CaSO_4$	67.0
$CaCO_3$	150

Table S6. K_d value of P5-CPN for the removal of iodine species in simulated wastewater.

Solid-liquid ratio	IO_3^-				I^-			
	Initial (mg L^{-1})	Final (mg L^{-1})	Removal (%)	K_d (mL g^{-1})	Initial (mg L^{-1})	Final (mg L^{-1})	Removal (%)	K_d (mL g^{-1})
0.5:1	1.13	1.02	9.30	2.15×10^2	0.77	0.07	90.91	2.14×10^4
1:1	1.13	0.78	30.94	4.48×10^2	0.77	0.05	93.51	1.35×10^4
2:1	1.13	0.56	50.47	5.08×10^2	0.77	0.03	96.10	1.23×10^4
5:1	1.13	0.32	72.12	5.06×10^2	0.77	0.01	98.70	1.29×10^4

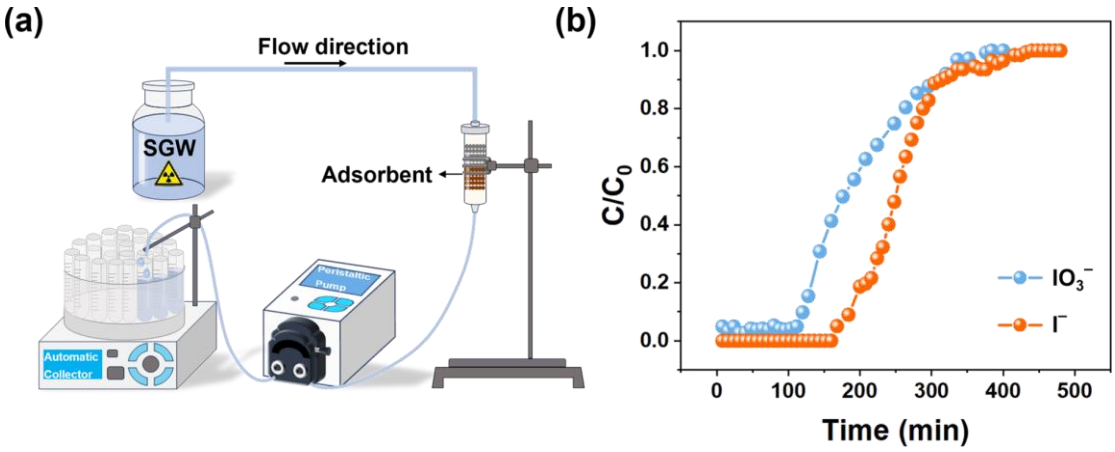

Fig. S20. (a) Experimental facility for dynamic IO_3^- and I^- removal by P5-CPN. (b) The concentration of IO_3^- and I^- at the outlet of simulated Hanford groundwater at different times during dynamic column adsorption (initial concentration: 1 ppm).

5. Adsorption mechanism

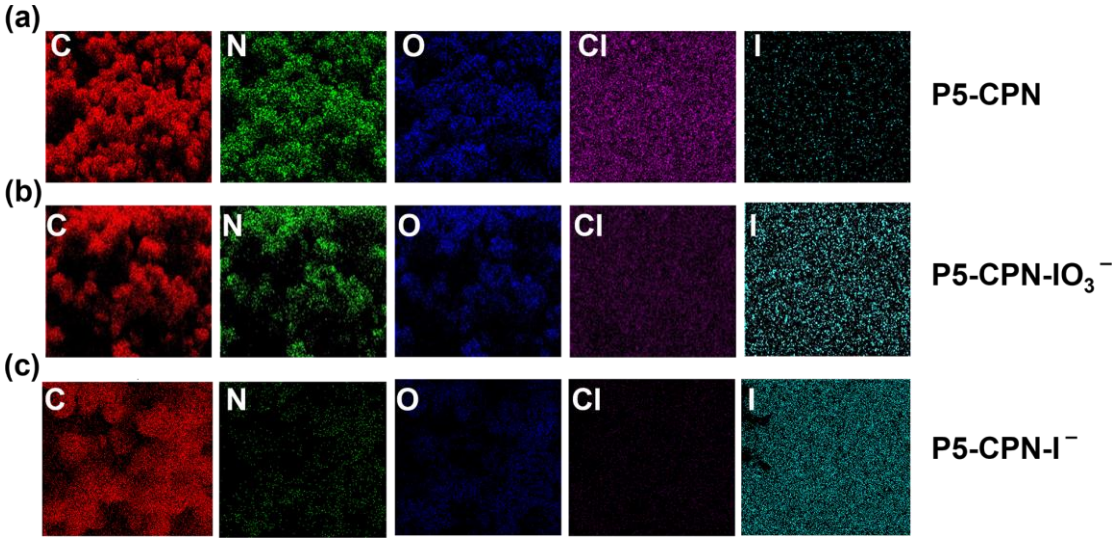

Fig. S21. SEM-EDS mapping of (a) P5-CPN, (b) P5-CPN-IO_3^-, and (c) P5-CPN-I^-.

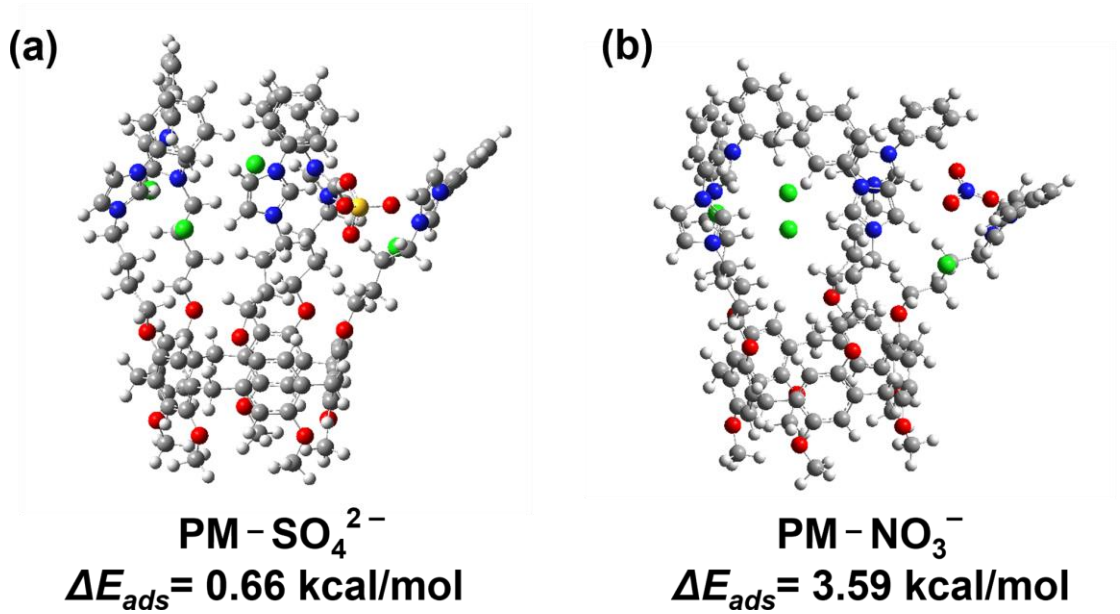

Fig. S22. The adsorption energies for SO_4^{2-} and NO_3^- with PM.

6. References

1. Q. Guo, J. Li, Y. Zhao, L. Li, L. He, F. Zhao, F. Zhai, M. Zhang, L. Chen, Z. Chai and S. Wang, *Angew. Chem., Int. Ed.*, 2024, **63**, e202400849.
2. C. I. Pearce, E. A. Cordova, W. L. Garcia, S. A. Saslow, K. J. Cantrell, J. W. Morad, O. Qafoku, J. Matyáš, A. E. Plymale, S. Chatterjee, J. Kang, F. C. Colon, T. G. Levitskaia, M. J. Rigali, J. E. Szecsody, S. M. Heald, M. Balasubramanian, S. Wang, D. T. Sun, W. L. Queen, R. Bontchev, R. C. Moore and V. L. Freedman, *Sci. Total Environ.*, 2020, **716**, 136167.
3. Gaussian 09, Revision E.01, M. J. Frisch, G. W. Trucks, H. B. Schlegel, G. E. Scuseria, M. A. Robb, J. R. Cheeseman, G. Scalmani, V. Barone, G. A. Petersson, H. Nakatsuji, X. Li, M. Caricato, A. V. Marenich, J. Bloino, B. G. Janesko, R. Gomperts, B. Mennucci, H. P. Hratchian, J. V. Ortiz, A. F. Izmaylov, J. L. Sonnenberg, Williams, F. Ding, F. Lipparini, F. Egidi, J. Goings, B. Peng, A. Petrone, T. Henderson, D. Ranasinghe, V. G. Zakrzewski, J. Gao, N. Rega, G. Zheng, W. Liang, M. Hada, M. Ehara, K. Toyota, R. Fukuda, J. Hasegawa, M. Ishida, T. Nakajima, Y. Honda, O. Kitao, H. Nakai, T. Vreven, K. Throssell, J. A. Montgomery Jr., J. E. Peralta, F. Ogliaro, M. J. Bearpark, J. J. Heyd, E. N. Brothers, K. N. Kudin, V. N. Staroverov, T. A. Keith, R. Kobayashi, J. Normand, K. Raghavachari, A. P. Rendell, J. C. Burant, S. S. Iyengar, J. Tomasi, M. Cossi, J. M. Millam, M. Klene, C. Adamo, R. Cammi, J. W. Ochterski, R. L. Martin, K. Morokuma, O. Farkas, J. B. Foresman and D. J. Fox, Gaussian, Inc., Wallingford CT, 2013.
4. W. J. Hehre, R. Ditchfield and J. A. Pople, *J. Chem. Phys.*, 1972, **56**, 2257-2261.
5. T. Clark, J. Chandrasekhar, G. W. Spitznagel and P. V. R. Schleyer, *J. Comput. Chem.*, 2004, **4**, 294-301.
6. L. Tu, C. Li, C. Liu, S. Bai, J. Yang, X. Zhang, L. Xu, X. Xiong and Y. Sun, *Chem. Commun.*, 2022, **58**, 9068-9071.
7. X. Yuan, Y. Cai, L. Chen, S. Lu, X. Xiao, L. Yuan and W. Feng, *Sep. Purif. Technol.*,

2020, **230**, 115843.
8. K. Zhang and T. Chen, *J. Environ. Radioact.*, 2018, **190-191**, 73-80.
9. K. Zhang and T. Chen, *J. Radioanal. Nucl. Chem.*, 2018, **316**, 543-551.
10. T. Da and T. Chen, *J. Radioanal. Nucl. Chem.*, 2020, **326**, 511-523.
11. Y. Zou, T. Chen, G. Yuan and K. Zhang, *J. Radioanal. Nucl. Chem.*, 2018, **317**, 723-730.
12. W. Yu, H. Xu, D. Tan, Y. Fang, E. E. Roden and Q. Wan, *Appl. Clay Sci.*, 2020, **184**, 105407.
13. K. Tokunaga, Y. Takahashi, K. Tanaka and N. Kozai, *Chemosphere*, 2021, **266**, 129104.
14. D. Li, D. I. Kaplan, A. Sams, B. A. Powell and A. S. Knox, *J. Environ. Radioact.*, 2018, **192**, 505-512.
15. W. Szczepaniak，H.Ko´scielna, *Anal. Chim. Acta*, 2002, **470**, 263-276.
16. S. Han, W. Um and W.-S. Kim, *Dalton Trans.*, 2019, **48**, 478-485.
17. D. Li, D. I. Kaplan, K. A. Price, J. C. Seaman, K. Roberts, C. Xu, P. Lin, W. Xing, K. Schwehr and P. H. Santschi, *J. Environ. Radioact.*, 2019, **208-209,** 106017.
18. T.-X. Da, T. Chen, W.-K. He, P. Liu, Y. Ma and Z.-F. Tong, *J. Radioanal. Nucl. Chem.*, 2021, **329**, 1277-1290.
19. J. Kang, T. G. Levitskaia, S. Park, J. Kim, T. Varga and W. Um, *Chem. Eng. J.*, 2020, **380**, 122408.
20. S. Liu, S. Kang, H. Wang, G. Wang, H. Zhao and W. Cai, *Chem. Eng. J.*, 2016, **289**, 219-230.
21. C. Yan, J. Li, C. Tan, G. Chen, Q. Zhao, Y. Chen, P. He, Y. Luo, T. Duan, J. Lei and L. Zhu, *ACS Appl. Mater. Interfaces*, 2023, **15**, 28135-28148.
22. Q. Zhao, G. Chen, Z. Wang, M. Jiang, J. Lin, L. Zhang, L. Zhu and T. Duan, *Chem. Eng. J.*, 2021, **426**, 131629.
23. V. Suorsa, M. Otaki, J. Virkanen and R. Koivula, *Int. J. Environ. Sci. Technol.*, 2021, **19**, 5155-5166.
24. J. Kang, F. Cintron-Colon, H. Kim, J. Kim, T. Varga, Y. Du, O. Qafoku, W. Um and T. G. Levitskaia, *Chem. Eng. J.*, 2022, **430**, 132788.
25. C. Copeman, H. A. Bicalho, M. W. Terban, D. Troya, M. Etter, P. L. Frattini, D. M. Wells and A. J. Howarth, *Chem. Commun.*, 2023, **59**, 3071-3074.
26. Y. Zhao, J. Li, L. Chen, Q. Guo, L. Li, Z. Chai and S. Wang, *J. Radioanal. Nucl. Chem.*, 2023, **332**, 1193-1202.
27. J. Kim, J. Kang and W. Um, *J. Environ. Chem. Eng.*, 2022, **10**, 107477.
28. D. Zhang, X. Y. Liu, H. T. Zhao, L. Yang, T. Lü and M. Q. Jin, *RSC Advances*, 2018, **8**, 21084-21091.
29. P. Mao, Y. Liu, Y. Jiao, S. Chen and Y. Yang, *Chemosphere*, 2016, **164**, 396-403.
30. P. Mao, L. Qi, X. Liu, Y. Liu, Y. Jiao, S. Chen and Y. Yang, *J. Hazard. Mater.*, 2017, **328**, 21-28.
31. L. Liu, W. Liu, X. Zhao, D. Chen, R. Cai, W. Yang, S. Komarneni and D. Yang, *ACS Appl. Mater. Interfaces*, 2014, **6**, 16082-16090.
32. T. Zhang, X. Yue, L. Gao, F. Qiu, J. Xu, J. Rong and J. Pan, *J. Cleaner Prod.*, 2017, **144**, 220-227.

33. W. Xu, W. Zhang, J. Kang and B. Li, *J. Solid State Chem.*, 2019, **269**, 558-565.
34. C. H. B. Ng and W. Y. Fan, *ChemNanoMat*, 2015, **2**, 133-139.
35. M. R. Zia, M. A. Raza, S. H. Park, N. Irfan, R. Ahmed, J. E. Park, J. Jeon and S. Mushtaq, *Nanomaterials*, 2021, **11, 588**.
36. L. Zhang and M. Jaroniec, *J. Colloid Interface Sci.*, 2017, **501**, 248-255.
37. X. Sha, H. Huang, S. Sun, H. Huang, Q. Huang, Z. He, M. Liu, N. Zhou, X. Zhang and Y. Wei, *J. Environ. Chem. Eng.*, 2020, **8**, 104261.
38. V. J. Inglezakis, A. Satayeva, A. Yagofarova, Z. Tauanov, K. Meiramkulova, J. Farrando-Pérez and J. C. Bear, *Nanomaterials*, 2020, **10**, 1156.
39. Z. Ye, L. Chen, C. Liu, S. Ning, X. Wang and Y. Wei, *React. Funct. Polym.*, 2019, **135**, 52-57.
40. J. Jang and D. S. Lee, *Sci. Total Environ.*, 2018, **615**, 549-557.
41. J. Chen, Q. Gao, X. Zhang, Y. Liu, P. Wang, Y. Jiao and Y. Yang, *Sci. Total Environ.*, 2019, **646**, 634-644.
42. J. Seon and Y. Hwang, *J. Hazard. Mater.*, 2021, **409**, 124415.